

This is the postprint version of the following article: Aboudzadeh MA, Sanromán-Iglesias M, Lawrie CH, Grzelczak M, Liz-Marzán LM, Schäfer T. Blocking probe as a potential tool for detection of single nucleotide DNA mutations: design and performance. *Nanoscale*. 2017;9(42):16205-16213. doi: [10.1039/C7NR06675A](https://doi.org/10.1039/C7NR06675A). This article may be used for non-commercial purposes in accordance with RSC for Self-Archiving.

Received 00th January 20xx,
Accepted 00th January 20xx

DOI: 10.1039/x0xx00000x

www.rsc.org/

Enhancement of detection of single nucleotide DNA mutations by short blocking probes: a comparative study in solution and on the surface

M. Ali. Aboudzadeh,^a M. Sanromán-Iglesias,^b C. H. Lawrie,^{c,e} M. Grzelczak,^{b,d,e} L. M. Liz-Marzán^{b,d,e} and T. Schäfer^{a,e}

The detection of single nucleotide DNA mutations associated with treatment decisions in cancer patients from liquid biopsies is a rapidly emerging area of personalized medicine that requires high specificity. Here we report an enzyme-free approach to detect the L858R mutation of *EGFR* that is a predictive biomarker of tyrosine kinase treatment in many cancers. This approach includes the addition of blocking probes with the antisense ssDNA at different blocking positions and different concentrations such as to avoid re-annealing with the respective sense ssDNA. The successful blocking strategy was corroborated by fluorescence spectroscopy in solution using two distinct FRET pairs and quartz crystal microbalance with dissipation (QCM-D) measurements under comparable experimental conditions, as the hybridization rate-limiting step in both methods is the nucleation process. The efficiency of hybridization of each blocking probe was strongly dependent on its position particularly when the analyte possesses a secondary hairpin-structure. We tested the performance of blocking probes in combination with gold nanoparticles; the obtained results were in agreement with those of QCM-D. These findings could facilitate the development of better biosensors, especially those using probes containing secondary structure.

Introduction

Complementary base-pair hybridization between short oligonucleotides as a blocking strategy plays a crucial role in designing DNA-based biosensors¹ and in polymerase chain reaction (PCR) primer design.^{2,3} The importance of DNA-based biosensors for detection of diseases, genome sequencing, forensics, and environmental control is increasing.⁴ Somatic mutational DNA-detection is particularly challenging as it requires the detection of trace amounts of specific DNA sequences often differing by a single nucleotide in a massive excess of non-mutated (i.e. wild-type) DNA sequence with mutated DNA sequences present at between 1000–100,000 copies per ml of blood.⁵ Although there have been various attempts at enriching these populations for the mutated dsDNA sequence by removal of wild-type dsDNA sequence (e.g. clamp-PCR, ARMS-PCR), to date there has been no attempt to enrich for ssDNA mutated sequences that is an essential feature of mutation detection based on non-PCR based hybridization techniques such as handheld or true point-of-care testing (POCT) devices.^{6,7}

Blocking strategies are required because in plasma, DNA exists in the form of dsDNA and is therefore not efficiently detected by binding probes. Consequently, for detection dsDNA requires denaturing, commonly by applying heat, to form ssDNA, as occurs in PCR. Nowadays, quantitative real-time PCR technology and digital PCR can determine gene duplications or deletions and melting

curve analysis immediately after PCR can identify small mutations, down to single base changes.^{8,9}

The aim of this work is to describe an approach that could create a simple platform for rapid detection of mutations in human DNA, combining an efficient blocking strategy with a sensitive detection by surface plasmon resonance of gold nanoparticles (AuNPs). As proof-of-principle, we focused on the L858R mutation in the epidermal growth factor receptor (*EGFR*) gene. Mutations in the *EGFR* gene are commonly found in several cancer types, and the mutations often result in altered expression and activity. It has been reported that over-expression of *EGFR* can result in uncontrolled cellular division which in turn accelerates tissue growth.^{10,11} Non-small cell lung cancers (NSCLC) are amongst the most common cancers in the world and are often associated with mutations in the *EGFR* gene. The presence of *EGFR* mutations such as L858R in NSCLC are FDA and EMA approved, predictive biomarkers of targeted therapies (tyrosine kinase inhibitors (TKIs)) such as Gefitinib, Erlotinib and Afatinib that have dramatically improved the outcome for NSCLC patients from a median overall survival (OS) <12 months with conventional chemotherapy to a median OS of 2–3 years.

We systematically studied the kinetic parameters of binding between complementary base-pair hybridization of antisense sequences either with blocking probes or sense sequences. To study the possible surface effects on the efficiency of the blocking probes, data were obtained both in solution using two distinct FRET pairs, and when one strand was covalently bound to gold sensor of the QCM-D. Few studies have attempted to investigate the efficiency of hybridization both in solution and on the surface.^{12,13} DNA blocking probes are currently applied in enzymatic genotyping of single-nucleotide polymorphisms (SNPs) in a microarray format and PCR-based techniques.¹⁴ Commonly, once dsDNA is denatured by heat, the excess of blocking probe accompanied by its short length kinetically favors the formation of the duplex between the blocking

^a Polymat, University of the Basque Country, 20018 Donostia-San Sebastián, Spain.

^b CIC biomaGUNE, Paseo de Miramón 182, 20009 Donostia-San Sebastián, Spain.

^c Molecular Oncology Group, Biodonostia Research Institute, 20014 Donostia-San Sebastián, Spain.

^d CIBER de Bioingeniería, Biomateriales y Nanomedicina (CIBER-BBN), 20009 Donostia-San Sebastián, Spain.

^e Ikerbasque, Basque Foundation for Science, 48013 Bilbao, Spain.

Electronic Supplementary Information (ESI) available: [details of any supplementary information available should be included here]. See DOI: 10.1039/x0xx00000x

probe and the antisense strand of the mutated DNA sequence upon cooling, instead of re-annealing of the latter with the sense strand to form dsDNA. Since all other DNA species will spontaneously re-anneal during cooling, the mixture becomes highly and specifically augmented for the sense strand of the mutated DNA sequence.¹⁵ This considerably reduces the possibility of non-specific binding of antisense to the mutated sense strand probe as well as possible interferences.

However, blocking is not straightforward when both the sense and antisense strand are capable of forming a secondary structure such as a hairpin. In this report, we therefore study the effect of secondary structures on hybridization kinetics demonstrating that it is of utmost importance to understand these structural effects when conceiving an optimum blocking strategy.

Experimental section

Materials and methods

10 mM phosphate buffered saline (PBS) containing 338 mM NaCl, 2.7 mM KCl, pH 7.4 at 25 °C. Immobilized TECP disulfide reducing gel (tris[2-carboxyethyl]phosphine hydrochloride) was purchased from Fisher Scientific. Note that TCEP was employed to cleave possible disulfides bond formed between oligomers.

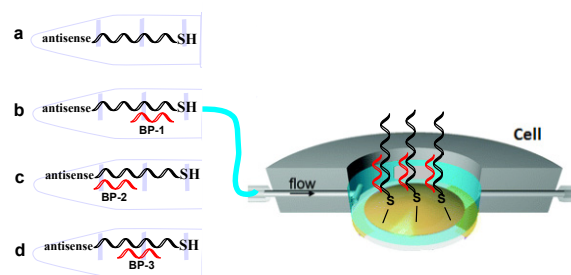
Oligonucleotides were synthesized and purified by HPLC (Biomers). The sequences used in this work are listed in **Table 1**. The 23mer oligonucleotide sense is a section of an EGFR L858R (T2573G) mutation in NSCLC. In QCM-D measurements, the sense strand was used without any label, while the antisense (the oligonucleotide complementary to the sense strand), labeled with a thiol group (thioctic acid) for immobilization on the gold sensors. For fluorescence spectroscopy measurements two FRET pairs were used; in the first pair, the sense strand was labeled with a black hole quencher (BHQ) at its 3'-end and the antisense strand was labeled with Atto488 dye at its 5'-end, while in the second pair we had BHQ dye at 5'-end position of sense strand and Atto488 dye at 5'-end position of the antisense strand. The selected 23mer antisense strand contains four base pairs involved in intramolecular folding (hairpin structure). The nucleobases participating in the secondary structure predicted by OligoAnalyzer 3.1 are underlined in **Table 1** for clarity.

Blocking probes were designed to bind to different sections of the antisense. Relative positions of the blocking oligos are shown in **Scheme 2**. As can be seen in this scheme, blocking probe 1 (BP1) was designed to be complementary to the 5'-half of antisense,

while blocking probe 2 (BP2) was designed to block the 3'-half of antisense. Blocking probe 3 (BP3) was designed to block the middle region of the antisense strand. For control experiments, the oligonucleotides BP1 and BP2 with BHQ label at 3'-end and 5'-end were used, respectively.

QCM-D measurements

Binding events were measured with a *Q-Sense Analyzer* system (Biolin Scientific / Q-Sense AB, Västra Frölunda, Sweden). Standard sensor chips (QSX301, Q-Sense, Västra Frölunda, Sweden) had the following specifications: frequency 4.95 MHz ± 50 kHz; diameter 14 mm; thickness 0.3 mm; RMS surface roughness of electrode <3 nm. Before immobilization of the ssDNA, the sensors were first cleaned with an UV-ozone cleaner (Bioforce) for 10 min, thereafter with Piranha base solution (1:1:5 ratio of H₂O₂, 25% ammonia solution, ultra-pure water, respectively) at 80 °C for 5 min, and again with UV-ozone treatment for 10 min. All QCM-D measurements were undertaken at 23 °C at a flow rate of 50 µL/min. Before each measurement, buffer was passed through the QCM-D flow module until obtaining a stable baseline. Prior to immobilization on gold sensors (QCM-D), thiolated antisense DNA was treated with TCEP disulfide reducing gel for 30 minutes prior to usage.



Scheme 1. Design of experiments: Five different case studies (**a**, **b**, **c** and **d**) were tested in QCM-D. As an example, the schematic immobilization of antisense strand on gold sensor in presence of BP1 is shown.

Five different combinations of TCEP-treated anti-sense at the concentration of 10 µM and a two-fold excess of blocking probes were prepared as shown in **Scheme 1** and incubated at room temperature for four hours. Each solution was injected in a separate experiment into the QCM-D chamber in order to form a stable Au-S monolayer which was evidenced by a sudden drop in the quartz crystal sensor frequency. Subsequently, the sensor was

Table 1. Sequence data of oligonucleotides.

Oligonucleotide	Sequence	T _m [°C] ^b
EGFR L858R Antisense 23mer	5'-GTTTGGCCCGCCCAAATCTGTG-3' ^a	
	5'-Atto488- GTTTGGCCCGCCCAAATCTGTG-3'	
	5'-GTTTGGCCCGCCCAAATCTGTG-Atto488-3'	64.9
	5'-Thioctic acid C6- GTTTGGCCCGCCCAAATCTGTG-3'	
EGFR L858R Sense 23mer	5'-CACAGATTTTGGGCGGGCCAAAC-3'	64.9

	5'-CACAGATTTTGGGCGGGCCAAAC-BHQ-3'	
	5'-BHQ-CACAGATTTTGGGCGGGCCAAAC-3'	
BP1	5'-GCGGGCCAAAC-3'	38
BP2	5'-CACAGATTTTGG-3'	34
BP3	5'-TTTTGGGCGGG-3'	36
CP1	5'-AAAATCTGTGTTTTTTTTTT- Thiol C6-3'	41
CP2	5'-Thiol C6-TTTTTTTTTTGTGGCCCGCCC-3'	63.4

^aNucleobases involved in the secondary structure predicted by OligoAnalyzer 3.1 are underlined.

^b T_m data are provided by supplier without taking into account modifications of the oligonucleotide (e.g. dyes, linkers).

^cOligonucleotides which were used for control experiments.

thoroughly rinsed with buffer such as to remove any non-binding ssDNA and then used for binding experiments. Finally, the 23-mer sense strand was injected and possible hybridization monitored until the frequency stabilized again. Non-binding sense strand was then flushed from the cell with buffer.

At least 2 independent experiments were carried out for each condition in order to calculate the averages and standard deviations presented in **Table 3**. Because the D factor is a ratio of energies, it is dimensionless and is reported as 10^{-6} dissipation units (DU).

Fluorescence and UV-Vis measurements

The fluorescence measurements were conducted employing a FS920 single photon counting spectrofluorimeter (Edinburgh Instruments, Scotland, UK) equipped with a 450 W xenon arc lamp using the kinetic scan mode at excitation of 480 nm and emission at 520 nm as well as the monochromator bandwidth at 3 and 6 nm, respectively. The temperature was controlled using the TApp Temperature Control Application software provided by the supplier.

For the experiments, carried out at 20 °C (well below T_m of duplex sense and antisense), the Atto488-labeled antisense was first added to the buffer solution placed in a quartz cuvette of 10 mm light path (Hellma), such as to yield a final concentration of 10 nM. Next, each of the blocking probes was added at concentrations equivalent to 10, 100 and 1000 nM. Finally, the BHQ-labeled sense strand was added such as to yield concentration of 10 nM. Before adding each oligomer into the cuvette, emission signal stability of the system was verified (± 100 counts). The kinetic measurements were repeated at least three times for every design under study. The kinetic curves were subsequently fit by a monoexponential growth model, and the hybridization rate constants were extracted by dividing the obtained constant by the sense strand concentration using OriginPro 8 (Origin Lab) software.

UV-Vis experiments were performed with a Varian Cary 5000 UV-Vis spectrophotometer equipped with a temperature controller and thermostated cell holder. Two-dimensional data (absorbance, temperature) were collected at 260 nm from 25 to 70 °C at 1 °C increments with a temperature ramp of 1 °C/min.

Hybridization kinetics were investigated by FRET. By monitoring the fluorescent signals over time through FRET, we determined the hybridization rate, k_h , according to, using the following equations:

$$F(t) = F_{\min} + (F_0 - F_{\min}) \cdot e^{-bt} \quad (\text{Eq. 1})^{16}$$

where: $F(t)$ is the fluorescence at time t , F_0 is the initial fluorescence value when the hybridization between two oligomers starts, F_{\min} is the normalized fluorescence value when the hybridization between the antisense and sense finishes and b is the hybridization rate constant obtained through curve fitting. Given the initial concentration of the sense strand the hybridization rate K_h between the two oligomers can be calculated from

$$b = [\text{sense}] \cdot K_h \quad (\text{Eq. 2})$$

Amplification by Au nanoparticles

Synthesis of Gold Nanoparticles (AuNPs)

AuNPs (63 nm) were synthesized following a seeded growth method¹⁷ that involved two steps: synthesis of seeds and growth. Synthesis of Au seeds: a solution of trisodium citrate (150 mL, 2.2 mM) was heated for 15 min under vigorous stirring until boiling, followed by injection of a solution of HAuCl₄ (1 mL, 25 mM). The color of the solution changed from yellow to bluish gray and then to light pink in 10 min. Seeded Growth: the seeded growth process comprised cyclic addition of metal precursor and extraction of particles product. In a typical process, the seed solution was cooled down to 90 °C and then HAuCl₄ solution (1 mL, 25 mM) was added, followed by a second addition after 30 min. After a further 30 min period, part of the growth solution (55 mL) was extracted and to the remaining solution (98 mL) water (53 mL) and sodium citrate (2 mL, 60 mM) were added. This addition/extraction process was repeated 5 times to obtain gold nanoparticles with 63 nm diameter (55 mL).

Functionalization of AuNPs

AuNPs were functionalized with thiolated oligonucleotides according to the method reported by Hurst *et al.*¹⁸. Briefly, to the AuNPs colloid (1.11 mL) containing SDS (0.1%) and PBS (0.01 M) was added a solution of oligonucleotides to reach a final concentration of 1 OD/mL. The mixture of oligonucleotides and AuNPs was incubated at room temperature for 20 min. To improve oligonucleotide binding onto the gold surface, a salt aging process was carried out. A solution containing NaCl (2 M), SDS (0.01%), and PBS (0.01 M) was added sequentially to the mixture containing AuNPs and oligonucleotides in the following aliquots: 5, 5, 15, 25,

and 50 μL , ultimately reaching a final NaCl concentration of 0.2 M. After each addition the mixture was sonicated for 10 s followed by a 20 min incubation period. The final solution was incubated for 12 h. To remove excess oligonucleotides, the solutions were centrifuged three times (8500 rpm for 10 min), each time redispersed in SDS (1 mL, 0.01%). The final concentration of nanoparticles was 0.4 mM in terms of metallic gold.

Hybridization of AuNP-DNA Probes

Blocking DNA was combined with the solution containing antisense strands in PBS (x1, 325 μL), and left undisturbed for 1h, followed by the addition of a mixture (50 μL) containing PB (0.01 M) and NaCl (2 M). Next, a solution containing sense strand was added to the above mixture, and left undisturbed for 15 min. The above solution was transferred to a UV-Vis mikro cuvette containing two batches of DNA-coated NPs (62.5 μL each). The final volume of the mixture was 0.5 mL, the concentrations of blocking, antisense and sense strands were 5 nM and the final concentration of NPs was 13 pM. Here, UV-Vis spectra were measured at room temperature on an Agilent 8453 UV-Vis spectrophotometer, using UV Micro cuvettes with 1 cm optical path length.

Results and discussion

The selected sequence for studying the blocking efficiency is the 23mer antisense strand of EGFR L858R (T2573G) mutation in NSCLC (non-small cell lung carcinoma). This 23mer undergoes a hairpin loop (Scheme 2) involving 15 of its bases at one extremity and leaving 7 bases dangling free on the other. The melting temperature of the hairpin structure predicted by OligoAnalyzer 3.1 (58 $^{\circ}\text{C}$) agrees qualitatively well with our experimental data obtained by curve fitting (61 $^{\circ}\text{C}$ in Fig. 1). The general lowest energy structure predicted by OligoAnalyzer 3.1 for this strand has a ΔG_{25}° value of -3.3 kcal/mol meaning that sense and antisense were most probably in a hairpin conformation prior to hybridization during our blocking experiments.

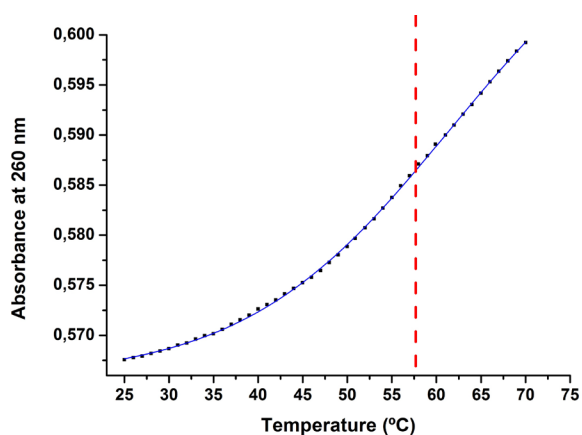
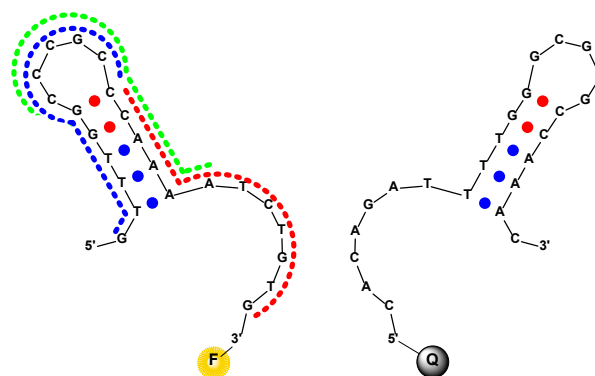


Fig. 1. Thermal melting of antisense strand monitored by UV absorbance spectroscopy. Melting curves shown were collected at a ramp rate of $1^{\circ}\text{C}/\text{min}$ for $1\mu\text{M}$ ssDNA in PBS. Red dashed line indicate the T_m predicted

by OligoAnalyzer 3.1 and blue line shows sigmoidal curve fitting with Boltzmann function.

The presence of this secondary structure means an energy penalty for hybridization not only between sense and antisense, but also for antisense and the blocking probe.



Scheme 2. Hairpin structure proposed by OligoAnalyzer 3.1 for second FRET pair: antisense (on the left) and sense (on the right) and respective binding positions of the blocking oligos, BP1 (blue color), BP2 (red color), and BP3 (green color).

We systematically designed blocking probes for studying the blocking of the 23-mer by equal-length oligonucleotides and depending on the docking region: BP1 and BP 3 would bind entirely to the hairpin region of the antisense and symmetrically cover overlapping but only partial regions of the hairpin. Except for one nucleotide (G and A, respectively), the nucleotides involved in the hybridization of BP1 and BP3, respectively, are therefore identical. They have been chosen for verifying whether it makes a difference for the blocking efficiency to be binding to one extremity of the antisense, or in the center region: for complete annealing of the sense and antisense, the hairpin structure must be disrupted. However, once the hairpin is disrupted BP3 may potentially be more efficient since it is placed in the middle region while BP1 would leave 7 consecutive nucleotides free for annealing. BP2 represents a very different blocking situation as it covers only partially the hairpin. Re-annealing of sense and antisense would therefore not only suffer from the energy penalty of the existing hairpin but also the fact that the only freely available sequence of the original structure is blocked by BP2. As can be seen from **Table 1**, the T_m values of the blocking probes were high enough to allow hybridization at room temperature under the reported buffer conditions.

In absence of any blocking probe, it would be expected that annealing of the sense and antisense strand would occur via the free 7mer sequence starting from the 3' position of the antisense, because full hybridization requires disrupting the internal hairpin. We therefore measured FRET with time for two situations: either with the fluorophore at the 5' of the antisense and the quencher at the 3' of the sense ("FRET pair 1"), or vice versa ("FRET pair 2").

As can be seen from **Table 2** in absence of any blocking probe, the apparent hybridization rate is 3.5-fold higher in the case of FRET

pair 2 compared to FRET pair 1. This corroborates the assumption that annealing of sense and antisense is penalized through the existence of the internal hairpin and therefore occurs starting from the free 7mer. We hypothesize that for complementary base-pair hybridization, the rate-limiting step is the formation of a transient intermediate with a few base pairs as a nucleation, which is then quickly followed by the rest of the bases forming a fully bound helix. This process applies to both random coil and hairpin DNA structures. Nucleation may occur at different sites¹⁹ and prefers to start from GC base pairs^{20,21}. Obviously, in our case the stem bases in hairpin structure of antisense strand cannot take part in nucleus formation. Except for these restricted bases, at 3'-end of our antisense strand, free bases may form nuclei when the length of continuous free bases is long enough (7 bases). Subsequently, once nucleation has occurred, full hybridization can only be achieved via disrupting the hairpin structure. Zhao et al. examined the effect of secondary structure on the kinetics mechanism of oligonucleotide hybridization via FRET and discovered that the large unfavorable enthalpy of hairpin structure melting is compensated by the favorable energy of associated partial duplex formation.²² Since FRET pair 2 is conjugated to the 7mer where annealing starts while FRET pair 1 is conjugated to the internal hairpin where annealing finalizes, the 3.5-fold increased measured hybridization rate of the former is only apparent and does not report any difference in overall hybridization as can be deduced from the steady-state binding efficiency measured in both cases and for all blocking probes, accounting for minor variations. Plotting hybridization rate acquired through the second FRET pair against the rates obtained by the first FRET pair yields a linear fit with a slope equal to 3.48, which confirms this hypothesis (Fig. S2).

The best blocking was obtained at 1000 nM of BP2 which reduced the hybridization of antisense and sense threefold from around 60% down to 20%. BP2 was significantly more efficient than BP1 and BP3, for which there could be two explanations: BP2 covers the only free 7mer and annealing of sense and antisense will be hindered by both BP2 and possibly remaining internal hairpins, or BP1 and BP3 do not bind efficiently to the antisense, at all, naturally resulting in a poor blocking. As can be seen in Table 2, even by Table 2. Values of normalized F_{\min} , K_h (error $\leq 0.001 \times 10^8 \text{ M}^{-1}\text{min}^{-1}$), and binding efficiency for hybridization of antisense with sense strand in presence of different concentrations of blocking probes.

increasing the concentration of BP1 up to 100 fold in the system, the hybridization of sense with antisense strand could not be prevented. In addition, the tendency of self-dimerization through internal GGCC bases of this blocking probe could be another reason for its inability to block by increasing concentration.

Comparing BP1 and BP3, which both need to disrupt the hairpin in order to anneal with the antisense, BP3 is slightly more efficient in blocking. Again, this efficiency might be due to a direct blocking or a simple consequence of BP3 binding more efficiently to the antisense than BP1. To clarify this doubt, we have studied the binding of each blocking probe to the antisense by QCM-D which has widely been employed to monitor DNA hybridization.^{23,24,25}

First, solutions of antisense and blocking probes showed in Scheme 1 (a, b, c and d) were incubated and then immobilized on the QCM sensor to form a monolayer of antisense strand in free or blocked state. Data in Table 3 illustrate that upon forming this monolayer, the frequency signal of QCM-D decreased between 27.6 (only antisense) to a maximum of 41.1 Hz in the case of BP2. Adsorbed mass of antisense (27.6 Hz) in absence of any blocking probe was considered as the reference and was used to calculate the binding efficiency of each blocking probe BP1, BP2 and BP3 during incubation process (b, c and d) and was obtained as 5%, 98% and 47%, respectively. Hence, this indicates that the high blocking efficiency observed for BP2 in Table 3 seems to be primarily due to the fact that BP2 bound more efficiently to the antisense than BP1 and BP3. The same applies for the difference observed between the latter two: BP1 binds rather poorly which naturally results also in a poor blocking efficiency (Table 3).

Subsequent injection of the sense solution allowed us to evaluate the blocking efficiency as was done for the data reported in Table 3, however, with the difference that blocking was studied with the antisense immobilized on a surface rather than being in solution. The comparison is relevant as solution data might not faithfully reflect those obtained from surface-immobilized systems owing to, for example, a reduced mobility or availability of binding sites in the former.

blocking probe (BP)	BP conc. [nM]	Fluorophore 5', Quencher 3' (FRET pair 1)			Fluorophore 3', Quencher 5' (FRET pair 2)		
		norm. F_{\min} [-]	K_h [$10^8 \text{ M}^{-1}\text{min}^{-1}$]	binding efficiency [%]	norm. F_{\min} [-]	K_h [$10^8 \text{ M}^{-1}\text{min}^{-1}$]	Binding efficiency [%]
none	-	0.40	0.155	60	0.35	0.541	65
BP1	10	0.47	0.130	53	0.35	0.377	65
	100	0.54	0.104	46	0.51	0.278	49
	1000	0.57	0.121	42	0.51	0.239	56
	10	0.46	0.038	54	0.61	0.064	39
BP2	100	0.53	0.036	47	0.59	0.049	41
	1000	0.80	0.034	20	0.80	0.057	20

	10	0.43	0.151	57	0.36	0.507	64
BP3	100	0.58	0.094	40	0.44	0.364	56
	1000	0.66	0.058	34	0.56	0.112	44

As can be seen in **Fig. S4** and data from **Table 3**, the sense strand hybridized with the antisense at a binding efficiency very similar to that observed in solution (**Table 2**, first row). Similarly, in the case of incubating antisense with BP2 (**c**), subsequent addition of sense strand resulted in a binding efficiency of 16% which is good agreement with the 20% observed in solution. Binding efficiency of sense strand to the layers AS+BP1 and AS+BP3 (experiments **b** and **d**, respectively) was obtained as 41 % and 28%, respectively, which also agreed qualitatively with the observations made in solution. It should be stressed that the AS-BP conjugates were formed in solution and subsequently immobilized such as to avoid experimental artefacts stemming from a reduced accessibility of binding sites very close to the sensor surface, e.g., as could be the case for BP1. Gooding *et al.* suggested that surface diagnostic methods such as QCM-D and SPR do not detect complete duplex hybridization, but instead, detect duplex nucleation.²⁶

These results confirmed that designed blocking probes could block the antisense with binding affinity in order of BP2 > BP3 > BP1 and confirmed that blocking data obtained in solution can be transferred to systems with surface-immobilized antisense, such as the AuNP system discussed below.

The QCM-D data also reveal that despite of both BP1 and BP3 binding to the same hairpin, BP1 is strongly hindered to do so. In any case, for both BP1 and BP3 not only blocking efficiency (= sense binding efficiency) is strongly dependent on the concentration of the blocking probes but also the apparent hybridization rate during

Table 3. Calculated mass and binding efficiency of DNA adsorbed through different test designs: anti-sense alone ($MW_{AS} = 7368 \text{ g}\cdot\text{mol}^{-1}$), anti-sense + BP1 ($MW_{BP1} = 3354 \text{ g}\cdot\text{mol}^{-1}$), anti-sense + BP2 ($MW_{BP2} = 3658 \text{ g}\cdot\text{mol}^{-1}$) and anti-sense + BP3 ($MW_{BP3} = 3417 \text{ g}\cdot\text{mol}^{-1}$). Average error for the frequency data is $\pm 0.6 \text{ Hz}$.

test design	Total ΔF [Hz]	absorbed Sauerbrey mass [ng cm ⁻²]	absorbed Sauerbrey moles [p mol cm ⁻²]	binding efficiency of BP to antisense [%]	sense strand ΔF [Hz]	binding efficiency of sense strand [%]
Antisense (AS)	27.6	488	66.3	-	14.4	55
AS + BP1	28.2	500	69.7	5	10.8	41
AS + BP2	41.1	727	131.5	98	4.2	16
AS + BP3	33.6	595	97.6	47	7.4	28

annealing of antisense and sense (**Table 2**). BP3 significantly decreased the hybridization rate only toward higher concentrations and at maximum 2.5-fold. In this case BP3 surrounds the hybridization sites (starting from the 7th base) and the frequency of successful collisions and subsequently the hybridization rate of the sense to the antisense are possibly reduced due to steric impairment of the binding sites. The hybridization rate is more severely affected when the only available site for target nucleation is next to the hairpin structure. As an example, changes in the fluorescence emission versus time for three blocking probes (BP1, BP2 and BP3) when they were added in equimolar amount with antisense are shown in **Fig. S1**.

This kinetic dependency on the blocking probe concentration follows the same trend for BP1 and BP3, even including the data point in absence of any blocking probe, but not so for BP2. **Fig. S3** reveals that the blocking efficiency of BP2 is hardly kinetically driven as it remains almost constant whatever the sense binding efficiency is and for both FRET pair 1 and 2.

QCM-D data comprise the measurement of the dissipation of a molecular layer immobilized on the sensor surface which in fact provides useful information on its viscoelastic properties that might eventually be correlated to the availability of binding sites. Such information is best extracted by plotting ΔD versus ΔF as it reports the change in dissipation for an incremental mass independent of time, and particularly for the case of DNA whose viscoelastic nature is due to the water associated to its chains.²⁷

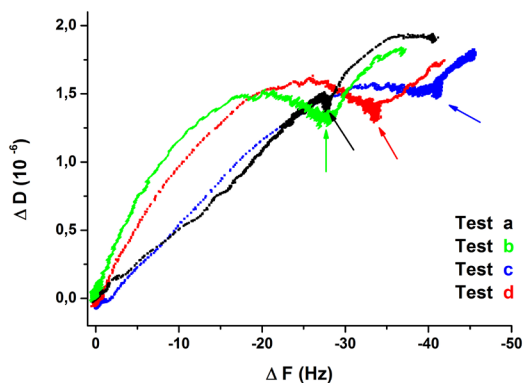


Fig. 3. Changes in dissipation ΔD vs. frequency changes ΔF , for the adsorption of the antisense alone ("Test a") and followed by binding of the three blocking probes, respectively ("Test b": BP1; "Test c": BP2; "Test d": BP3). Arrows in the Fig. indicate the points at which the sense strand was added to each of the samples.

Fig. 3 reveals that the conjugates antisense+BP1 and antisense+BP3 on one hand, and antisense alone and antisense+BP3 immobilize in a similar manner, respectively, and first with the latter clearly less dissipative than the former. However, these initially more dissipative conjugates comprising BP1 and BP3, respectively, subsequently undergo a pronounced rearrangement toward the steady-state of the immobilization. Before adding the sense strand (arrow in **Fig. 3**), this rearrangement yields $\Delta D/\Delta F$ values of about $5.2 \times 10^{-5} \text{ Hz}^{-1}$ for both antisense and antisense+BP1, $3.4 \times 10^{-5} \text{ Hz}^{-1}$ for antisense+BP2 and $4.2 \times 10^{-5} \text{ Hz}^{-1}$ for antisense+BP3. Hence, the highest dissipative layer is observed for the antisense with the internal hairpin structure, and the fact that antisense+BP1 yields the same value corroborates the very minor binding of BP1 reported in **Table 3**. The $\Delta D/\Delta F$ values BP2 and BP3 are in line with this consideration. Subsequent binding of the sense strand (after the arrow in **Fig. 3**) occurs with a similar increase in

dissipation per unit frequency (mass adsorbed) and eventually yields $\Delta D/\Delta F$ values around $4.5 \times 10^{-5} \text{ Hz}^{-1}$ for all conjugates except the one involving BP2 which amounts to a slightly lower $3.9 \times 10^{-5} \text{ Hz}^{-1}$.

Performance of blocking probes with Au nanoparticles

Finally, we evaluated the performance of each blocking probe in the process of DNA-triggered aggregation of gold nanoparticles. We functionalized spherical gold nanoparticles (64 nm) with capture probes to obtain two batches of nanoparticles. The solutions containing gold nanoparticles displayed a localized surface plasmon resonance (LSPR) band with the maximum at 538 nm (see **Fig. S5**). The initially stable solution of nanoparticles underwent aggregation in the presence of sense sequence that is complementary to capture probes stabilizing both types of nanoparticles (**Fig. 4e**). The aggregation process caused the changes of the optical properties that is manifested by the broadening of the LSPR band and emergence of a new band at 620 nm (see Supporting information). To monitor the aggregation process, we used UV-Vis spectroscopy that allowed us to estimate the aggregation rate - the ratio of the absorbance at 620 nm and 638 nm. Therefore, the maximum aggregation rate was observed for the mixture containing nanoparticles and sense sequences (**Fig. 4e**). In contrast, the minimum aggregation rate was noted in the case of the mixture containing gold nanoparticles together with sense and antisense couple, since the double strands comprising sense and antisense excluded the bridging of the nanoparticles with the sense sequence (**Fig. 4a**).

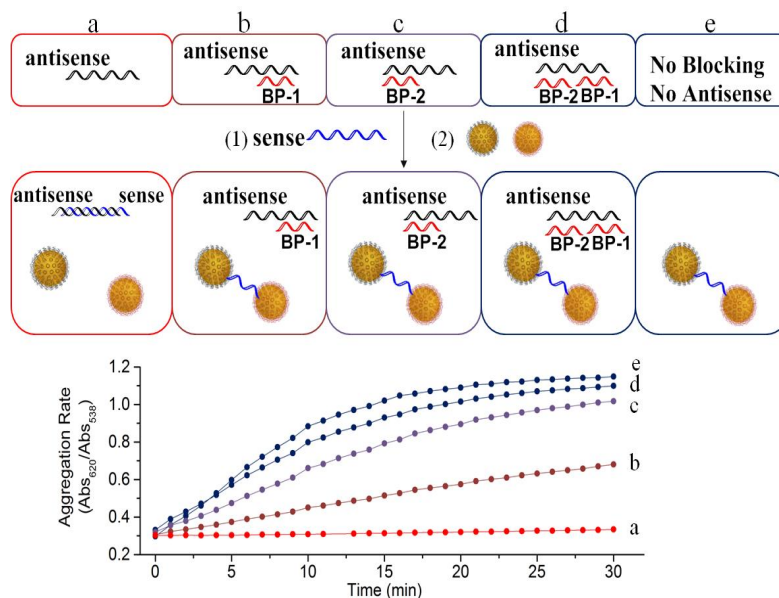


Fig. 4. Efficiency of blocking probes in the selective aggregation of Au nanoparticles. (Upper) Schematic diagrams of the performed experiments. Antisense sequences were mixed with the corresponding blocking probes and subsequently subjected to the sense sequence and colloidal solution of gold nanoparticles. (a, e) Control experiments, (b, c, d) blocking of antisense by BP1, BP2, and the mixture of BP1 and BP2. (Lower) Aggregation rate vs. aggregation time for different blocking probes and control experiments.

The aggregation rate is correlated with blocking ability, to test the blocking probe's efficiencies; we premixed the antisense strands with different blocking probes: BP1, BP2 and the combination of both. The use of two blocking probes (BP1 and BP2) inhibited the hybridization of the sense and antisense sequences (**Fig. 4d**), allowing the sense sequence to bridge the nanoparticles, hence increasing the aggregation rate. Comparative experiments showed that BP2 blocks improve the formation of double strand (sense-antisense) than BP1. The aggregation rate for BP2 was almost double as compared to the case of BP1 (compare **Fig. 4c** and **4b**). Although BP1 exhibits a certain blocking ability, these results are in agreement with those obtained by QCM-D and in solution.

Conclusions

We systematically studied the binding efficiency of sense strand to antisense in absence and in presence of three different blocking probes in both surface and solution-phase environments. Our comparison was based on measurements from two techniques, FRET measurements with hybridization occurring in solution and QCM-D measurements with the antisense strand immobilized on a surface. We validated our observations with an actual application based on the agglomeration of gold nanoparticles.

We have shown that a secondary structure present in the antisense single strand can significantly suppresses the binding efficiency of a blocking probe and consequently the efficiency in avoiding re-annealing of antisense and sense strand. Hence, blocking probe efficiency becomes in fact more dependent on the binding position rather than the concentration. DNA hybridization was studied in solution by FRET as well as with the antisense immobilized on a sensor surface by QCM-D. While the data were qualitatively in agreement, attention has been drawn to the need to carefully choose the position of the FRET pairs when determining the kinetics of DNA hybridization in presence of internal secondary structures as this can affect strongly the hybridization rates observed. The observations made should help the systematic design of bioanalytical flow devices for detection of DNA strands where the kinetics of annealing and blocking are fundamental.

Acknowledgements

CIC biomaGUNE acknowledges the projects MAT2013-49375-EXP and MAT2013- 46101-R. This work was also supported by Excelencia Instituto Carlos III grant (project No. PIE13/00048).

Notes and references

1 T. G. Drummond, M. G. Hill and J. K. Barton, *Nat.*

- 2 *Biotechnol.*, 2003, **21**, 1192–1199.
- 3 J. M. S. Bartlett and D. Stirling, Eds., *PCR Protocols*, Humana Press, 2003, vol. 226.
- 4 T. Yamada, H. Soma and S. Morishita, *Nucleic Acids Res.*, 2006, **34**, 665–669.
- 5 K. M. Abu-Salah, M. M. Zourob, F. Mouffouk, S. A. Alrokayan, M. A. Alaamery and A. A. Ansari, *Sensors (Switzerland)*, 2015, **15**, 14539–14568.
- 6 E. Gormally, E. Caboux, P. Vineis and P. Hainaut, *Mutat. Res. - Rev. Mutat. Res.*, 2007, **635**, 105–117.
- 7 A. Niemz, T. M. Ferguson and D. S. Boyle, *Trends Biotechnol.*, 2011, **29**, 240–250.
- 8 A. St John and C. P. Price, *Clin. Biochem. Rev.*, 2014, **35**, 155–67.
- 9 P. S. Bernard and C. T. Wittwer, *Clin. Chem.*, 2002, **48**, 1178–1185.
- 10 C. A. Milbury, Q. Zhong, J. Lin, M. Williams, J. Olson, D. R. Link and B. Hutchison, *Biomol. Detect. Quantif.*, 2014, **1**, 8–22.
- 11 S. Dearden, J. Stevens, Y. L. Wu and D. Blowers, *Ann. Oncol.*, 2013, **24**, 2371–2376.
- 12 M. Ladanyi and W. Pao, *Mod. Pathol.*, 2008, **21**, S16–S22.
- 13 Y. Gao, L. K. Wolf and R. M. Georgiadis, *Nucleic Acids Res.*, 2006, **34**, 3370–3377.
- 14 M. M. A. Sekar, W. Bloch and P. M. St John, *Nucleic Acids Res.*, 2005, **33**, 366–375.
- 15 M. P. Johnson, L. M. Haupt and L. R. Griffiths, *Nucleic Acids Res.*, 2004, **32**, e55.
- 16 R. Wang, M. Minunni, S. Tombelli and M. Mascini, *Biosens. Bioelectron.*, 2004, **20**, 598–605.
- 17 M. Tsuruoka, K. Yano, K. Ikebukuro, H. Nakayama, Y. Masuda and I. Karube, *J. Biotechnol.*, 1996, **48**, 201–8.
- 18 J. Comenge and V. Puentes, 2011, 11098–11105.
- 19 and C. A. M. Sarah J. Hurst, Abigail K. R. Lytton-Jean, *Anal. Chem.*, 2008, **78**, 8313–8318.
- 20 M. E. Craig, D. M. Crothers and P. Doty, *J. Mol. Biol.*, 1971, **62**, 383–392.
- 21 D. Pörschke, O. C. Uhlenbeck and F. H. Martin, *Biopolymers*, 1973, **12**, 1313–1335.
- 22 J. A. Subirana and P. Doty, *Biopolymers*, 1966, **4**, 171–187.
- 23 C. Chen, W. Wang, Z. Wang, F. Wei and X. S. Zhao, *Nucleic Acids Res.*, 2007, **35**, 2875–2884.
- 24 E. Huang, M. Satjapipat, S. Han and F. Zhou, *Langmuir*, 2001, **17**, 1215–1224.
- 25 R. Lao, S. Song, H. Wu, L. Wang, Z. Zhang, L. He and C. Fan, *Anal. Chem.*, 2005, **77**, 6475–6480.
- 26 F. Caruso, E. Rodda, D. N. Furlong, K. Niikura and Y. Okahata, *Anal. Chem.*, 1997, **69**, 2043–2049.
- 27 E. L. S. Wong, E. Chow and J. J. Gooding, *Langmuir*, 2005, **21**, 6957–6965.
- 28 F. Höök, A. Ray, B. Nordén and B. Kasemo, *Langmuir*, 2001, **17**, 8305–8312.